Atmos. Chem. Phys. Discuss., 15, 17711–17742, 2015
www.atmos-chem-phys-discuss.net/15/17711/2015/
doi:10.5194/acpd-15-17711-2015

Atmospheric Chemistry and Physics
Discussions

Assessment of multi-decadal WRF-CMAQ simulations for understanding direct aerosol effects on radiation "brightening" in the United States

C.-M. Gan[1], J. Pleim[1], R. Mathur[1], C. Hogrefe[1], C. N. Long[2], J. Xing[1], D. Wong[1], R. Gilliam[1], and C. Wei[3]

[1]Atmospheric Modeling and Analysis Division, National Exposure Research Laboratory, US Environmental Protection Agency, Research Triangle Park, NC, USA
[2]Cooperative Institute for Research in Environmental Sciences (CIRES), University of Colorado Boulder and NOAA, Boulder, CO, USA
[3]Max Planck Institute for Chemistry, Mainz, Germany

Received: 18 May 2015 – Accepted: 10 June 2015 – Published: 01 July 2015

Correspondence to: C.-M. Gan (gan.meei@epa.gov, chuenmeei@gmail.com)

Published by Copernicus Publications on behalf of the European Geosciences Union.

Abstract

Multi-decadal simulations with the coupled WRF-CMAQ model have been conducted to systematically investigate the changes in anthropogenic emissions of SO_2 and NO_x over the past 21 years (1990–2010) across the United States (US), their impacts on anthropogenic aerosol loading over North America, and subsequent impacts on regional radiation budgets. In particular, this study attempts to determine the consequences of the changes in tropospheric aerosol burden arising from substantial reductions in emissions of SO_2 and NO_x associated with control measures under the Clean Air Act (CAA) especially on trends in solar radiation. Extensive analyses conducted by Gan et al. (2014) utilizing observations (e.g. SURFRAD, CASTNET, IMPROVE and ARM) over the past 16 years (1995–2010) indicate a shortwave (SW) radiation (both all-sky and clear-sky) "brightening" in the US. The relationship of the radiation brightening trend with decreases in the aerosol burden is less apparent in the western US. One of the main reasons for this is that the emission controls under the CAA were aimed primarily at reducing pollutants in areas violating national air quality standards, most of which were located in the eastern US while the relatively less populated areas in the western US were less polluted at the beginning of this study period. Comparisons of model results with observations of aerosol optical depth (AOD), aerosol concentration, and radiation demonstrate that the coupled WRF-CMAQ model is capable of replicating the trends well even through it tends to underestimate the AOD. In particular, the sulfate concentration predictions were well matched with the observations. The discrenpancies found in the clear-sky diffuse SW radiation are likely due to several factors such as potential increase of ice particles associated with increasing air traffic, the definition of "clear-sky" in the radiation retrieval methodology and aerosol semi-direct and/or indirect effects which cannot be readily isolated from the observed data.

1 Introduction

Sulfate and nitrate are important secondary aerosols as they are key contributors to the airborne $PM_{2.5}$ (particulate matter that is 2.5 micrometers in diameter and smaller) mass in the United States (US) (Hand et al., 2012, 2013 and Blanchard, 2013). Because of its adverse impact on human health and ecosystem, surface-level $PM_{2.5}$ is extensively monitored to determine compliance with the particulate matter National Ambient Air Quality Standards (NAAQS). Moreover, knowledge of the alteration in the net radiative flux associated with the change of anthropogenic aerosol concentrations is essential to better understand aerosol radiative forcing and its effect on Earth's radiation budget (Chin et al., 2014; IPCC, 2014a, b). For example, radiation brightening is the gradual increase in the amount of shortwave irradiance at the Earth's surface which has been affected by changes in atmospheric constituents such as anthropogenic aerosol and cloudiness. In a recent study, Gan et al. (2014a) showed the effects of the implementation of controls under the Clean Air Act (CAA) on changing anthropogenic aerosols burden and associated radiation brightening in the US. This extensive analysis of various observation networks over the past 16 years (1995–2010) indicated that both all-sky and clear-sky shortwave (SW) radiation have experienced "brightening" in the US especially in the east region (Wild et al., 2009; Long et al., 2009; Augustine and Dutton, 2013). It however remains challenging to quantify the aerosol SW radiative forcing solely based on measurements since the distribution, life time and sources of anthropogenic aerosol are irregular in space and time. Here we extend our previous analysis (Gan et al., 2014a) by using the two-way coupled Weather Research and Forecasting (WRF) – Community Multi-scale Air Quality (CMAQ) model (Wong et al., 2012) to further investigate the changing aerosol effects on radiation "brightening". This study is also an assessment of the ability of the coupled model to replicate the observed trends of SW radiation, particulate matter and aerosol optical depth utilizing a comprehensive emission dataset (Xing et al., 2013).

Section 2 gives a brief overview of each observation network together with their measurements. The configurations of the coupled model together with methodologies that are applied to each dataset are also briefly discussed in this section. The results from the analyses of these datasets are presented in Sect. 3. In this section, the effects of the reduction in SO_2 and NO_x emissions on the radiation budget are assessed by using observed and modeled AOD and surface-level particulate matter. In addition, observed and modeled all-sky and clear-sky downwelling SW radiation are compared to further investigate trends in the aerosol direct effect. In Sect. 4 we summarize the findings and conclusions from our analyses.

2 Dataset

2.1 Observations

Data from several observational networks including SURFRAD (Surface Radiation Budget Network), Atmospheric Radiation Measurement (ARM), CASTNET (Clean Air Status and Trend Network) and IMPROVE (Interagency Monitoring of Protection Visual Environments) from 1995 to 2010 are used in this study for comparison with model results across the US. The six sites from SURFRAD and one site from ARM, listed in Table 1 and shown in Fig. 1, are the main focus in this study. They are paired with the closest sites from CASTNET and IMPROVE with the longest available measurements within the simulation period. Note that some sites are farther away from the SURFRAD sites while some are closer (see "Distance" in Table 1 for more information). For example, the Bondville group has all 3 sites (SURFRAD, CASTNET and IMPROVE) colocated while the Goodwin Creek group has the IMPROVE site ~ 500 km away from the SUFRAD site. Measurements of interests are SW radiation, aerosol composition concentrations near the surface and aerosol optical depth (AOD). In this study, we required data completeness of 80 % or greater for each individual year to minimize any artificial effects on inferred seasonal variations and trends. This criterion was met for each year at all sites for the time periods listed in Table 1. For example, observed AOD is only available after 1997 so the trends comparison spans 1997–2010 instead of 1995–2010. Additional details on the quality of the data and the methodology used to process each dataset can be found in Gan et al. (2014a).

2.2 Weather Research and Forecasting (WRF) – Community Multi-scale Air Quality (CMAQ) model

The coupled two-way WRF-CMAQ (Wong et al., 2012) model simulations were performed with a configuration based on coupling WRFv3.4 and CMAQv5.0.2. For this study, the output temporal resolution is one hour while the modeling domain covering the Continental US (CONUS) (see Fig. 1) is discretized with grid cells of size 36 by 36 km in the horizontal and with 34 vertical layers of varying thickness (between the surface and 50 mb). Two sets of simulations (with aerosol feedback (FB) and without aerosol feedbacks (NFB)) are performed from 1990 to 2010. Note that the aerosol feedback simulation involved only the direct aerosol effects on radiation and photolysis. In these feedback simulations, aerosol effects are treated dynamically where the CMAQ chemistry and radiation feedback modules are called every 5 and 20 time steps of WRF correspondingly. While the time step of WRF is 60 s, the meteorology fields are updated from the feedback module every 20 min. Additionally, only the analysis of the last 16 years (1995–2010) is discussed since most of the measurements of interest are available starting in 1995. Four Dimensional Data Assimilation (FDDA) based on National Centers fior Environmental Prediction (NCEP) Automated Data Processing (ADP) Operation Global Surface Observation (http://rda.ucar.edu/datasets/ds464.0/ last access 10 June 2015) and NCEP ADP Global upper Air observational Weather Data (http://rda.ucar.edu/datasets/ds351.0/#!description, last access 10 June 2015) is applied above the PBL using nudging coefficients of wind (guv), temperature (gt) and moisture (gq) (i.e. guv = $0.00005\,\mathrm{s}^{-1}$, gt = $0.00005\,\mathrm{s}^{-1}$ and gq = $0.00001\,\mathrm{s}^{-1}$) (Stauffer and Seaman, 1994; Pleim and Xiu, 2003; Pleim and Gilliam, 2009). These nudging coefficients are lower than the typical values used in standard WRF-CMAQ simulations in order to minimize the masking of the aerosol direct feedback effects (difference between feedback and no feedback runs). Hogrefe et al. (2015) showed that these minimal nudging coefficients had very little effect on the magnitude of the aerosol direct feedback effects compared to sensitivity simulations where no nudging was used. The comprehensive emission data used in this simulation is based on Xing et al. (2013) and time varying chemical lateral boundary conditions were obtained from a 108 km × 108 km WRF-CMAQ hemispheric simulation (Xing et al., 2015). The details of the model parameterizations are listed in Table 2.

2.3 Data analysis methodology

First, the seven sites shown in Fig. 1 are separated into east and west regions. The results from each observation network are presented as time series of their network mean of eastern US (i.e. averaging the annual mean of BON, GWN, PSU and SGP to obtain the eastern network mean) and of western US (i.e. averaging the annual mean of TBL, FPK and DRA to obtain the western network mean). Note that they are shown as annual mean anomalies except AOD. The same averaging technique is applied to the model output and emission dataset. Model data is extracted from the grid cell where the site is located. After that, least square fits (LSF) are applied to both eastern and western network means for observations, model output and emissions to determine the trends individually.

To ensure the estimated trends are statistically significant, a regression analysis is used to account for autocorrelation and variability in both observed and modeled data. This statistical methodology is constructed from Weatherhead et al. (1998); the general principle and its application are briefly discussed in the following paragraph.

After calculation of the annual mean for each dataset, each trend is estimated as the slope coefficient (m) of the LSF. Assuming a simple linear model,

$$Y_t = mX_t + c + N_t \quad (1)$$

where Y_t is the observed value at time t, c is the intercept term, m is the slope, X_t is year t of the time series and N_t is the noise of the time series (i.e. residual from the straight-line fit at time t). This noise term is assumed to be autoregressive with a lag of one time period (i.e. $N_t = \phi N_{t-1} + \varepsilon_t$, where ϕ is the autocorrelation coefficient and ε_t are independent and identically distributed random variables with mean zero, and variance σ_ε^2). Once the m has been estimated using generalized least squares regression (i.e. $\hat{m}$), the standard deviation of $\hat{m}$ can be estimated by:

$$\sigma_m \approx \frac{\sigma_N}{t^{\frac{3}{2}}}\sqrt{\frac{1+\phi}{1-\phi}} \tag{2}$$

where σ_N is the standard deviation of the noise parameter N_t, and t is the number of years. The significance of the trend can be calculated using the ratio $\frac{|\hat{m}|}{\sigma_m}$, i.e. the absolute trend relative to its uncertainty estimate. This ratio is assumed to be approximately normally distributed with mean zero and standard deviation 1. Thus, if this ratio is 1.96 or greater, the trend is significant at the 95 % confidence level. In the same way, if this ratio is greater than 1.65, the trend is significant at the 90 % confidence level. The term "significant" in this study represents the estimated trend is statistically significantly different from zero at the given confidence level. Note that it becomes more difficult to identify a trend with a given level of confidence as σ_m increases.

In addition to the time series and trends at specific modeling locations, our analysis also includes maps of trends in annual mean values calculated from the 1995–2010 WRF-CMAQ simulations over the CONUS domain overlaid with circles representing observed trends from the seven selected sites for each network. The size of the circle represents the level of the significance (e.g. the bigger the circle, the higher the significance). Analysis of the entire US for the entire 16 years period (except AOD is represented by the last 14 years) provides a better overall understanding of the spatial extent of the effects of the CAA implementation across US than just the seven groups of sites.

3 Results

3.1 Trends in aerosol concentrations

Since this study attempts to determine the aerosol radiative effects, the following discussion focusses only on the feedback simulations. First, the observed and modelled surface aerosol concentrations are assessed at the CASTNET and IMPROVE monitors. Their time series trends are presented in Figs. 2 and 3 respectively. As illustrated in Fig. 2a–f, the locations of the CASTNET monitors in the western US show small decreasing or almost no trends in observations, model, and emissions for all species (i.e. sulfur dioxide, SO_2; sulfate, SO_4^{2-}; nitrate, NO_3^-) while more dramatic decreasing trends are noted at the eastern US sites. This finding is not surprising because the implementation of the CAA reduced emissions and consequently ambient air pollutants in source regions predominantly located in the eastern US (e.g. targeted at areas exceeding the NAAQS). In contrast air pollution concentrations were low at the rural western monitors from the beginning resulting in the noted weaker trend (Gan et al., 2014a). Therefore, more dramatic decreasing trends are observed in the eastern US. The calculated trends are summarized in Table 3. In general, the results listed in this table show that the model output and emissions agreed well with CASTNET measurements (i.e. decreasing trends). In Fig. 3a–f and Table 4, similar trends (i.e. decreasing or almost no trend) are observed in measurements, model output, and emissions for SO_4^{2-}, NO_3^- and EC at the IMPROVE monitors locations. Overall, the model predictions agree well with surface measured aerosol concentration for both networks, especially SO_4^{2-}. This demonstrates that the coupled WRF-CMAQ model is able to replicate the long-term trends of anthropogenic aerosol loadings well, thereby providing confidence for examining trends in aerosol direct effects.

To assess the effects of reduction in anthropogenic emissions resulting from the implementation of the CAA during 1995–2010, the modelled trends in annual means across the entire CONUS domain for all species are presented in Fig. 4a–f along with observed trends at the seven sites (color coded circles) from the CASTNET and

IMPROVE networks. In general, at the location of observations (circles), the modeled and observed trends agree well in direction and magnitude. As shown in the Fig. 4a–f, more substantial reductions are noted in the eastern US, in particular for sulfate. Again this result validates previous findings and indicates there is a possibility of aerosol direct effect induced “brightening” in the US over the past 16 years (Gan et al., 2014a).

Before examining the total AOD, the $PM_{2.5}$ concentrations from IMPROVE are evaluated to gain some insight into the change in the total particulate matter burden resulting from air pollution controls. In particular, decreasing trends in $PM_{2.5}$ should be indicative of trends in the AOD and consequently trends in aerosol direct effects. In Fig. 5a and b, time series of annual mean $PM_{2.5}$ from observations (blue line) and model simulations (red line) are presented together with c a map of the modeled and observed trends across the entire CONUS domain. Observed and modeled trends are well matched with each other (see Table 4). A small or almost no trend is seen in the western US while a dramatic decreasing trend is evident in the eastern US and illustrates the effectiveness of air pollution controls strategies in improving the air quality over large portions of the US.

3.2 Trends in aerosol optical depth (AOD) and SW radiation

As a result of the reduction in the tropospheric particulate matter burden, the AOD was reduced in the eastern US over the 14 year period (1997–2010) as illustrated in Fig. 6a–c. However, the AOD in the western US shows very little change over this period. Even though the model predicted AOD is underestimated relative to the observations (see Fig. 6a, b and Table 5), the model is still able to capture trends similar to observations (obs_west: 0.0009 year^{-1}, sim_west: 0.0001 year^{-1} and obs_east: −0.0012 year^{-1}, sim_east: −0.0017 year^{-1}). One of the possible reasons for the model underestimation maybe due to the insufficient of emission sources in the model input such as sea salt, wild fires and underestimation of secondary constituents such as secondary organic aerosols (Gan et al., 2014b; Curci et al., 2014).

As discussed by Gan et al. (2014a), the “brightening” effects are evident in the observed all-sky and clear-sky total SW radiation trends and this finding was confirmed for all-sky by the model results as illustrated in Fig. 7a and b and less so for the clear-sky shown in Fig. 8a and b. Stronger and better agreement is noted in the all-sky SW radiation trend (see Fig. 9a and Table 5) while there is a weaker model trend and less agreement in the clear-sky SW radiation (see Fig. 9b and Table 5). One of the possible causes for this underestimate in model trend in the all-sky total SW radiation can be due to the cloud and the lack of representation of aerosol indirect effects in the current model simulations. Aerosol indirect effects have recently been included in the WRF-CMAQ model (Yu et al., 2015), and the effects on the radiation will be investigated in a future study. The trend of the clear-sky SW radiation from the model is underestimated compared to the observations and the opposite in trend for the direct and diffuse components separately especially for the East. One of the potential causes of this underestimate maybe related to the underestimation of particulate matter concentration and AOD. Another possible source of disagreement between modelled and observed trends in the clear-sky direct and diffuse components is not accounting for possible clear-sky sky “whitening” proposed by Long et al. (2009) and mentioned by Gan et al. (2014a) which acts to repartition the downwelling SW from the direct into the diffuse field (see further discussion below). However, as can be seen in Fig. 8b, the model trends in clear-sky total SW agree in the aggregate with the eastern SURFRAD sites over the last 11 years (i.e. clear-sky SW 2000–2010 trends for obs_east: 0.3055 $\text{W}\,\text{m}^{-2}\,\text{year}^{-1}$, sim_east: 0.1905 $\text{W}\,\text{m}^{-2}\,\text{year}^{-1}$). Similar finding was found in the AOD 11 years (2000–2010) trend (obs_east: −0.0026, sim_east: −0.0019). The 1995–2010 eastern SURFRAD trend is strongly influenced by two anomalous years (1998 and 1999). These anomalies are likely associated with the very strong El Nino occurrence of 1998–1999 which had significant impact on continental US weather patterns, and the model’s poor agreement with the observations for these years may also be due errors in the model representation of emissions and associated AODs since the emission estimates for earlier years likely are more uncertain than the estimates for more recent years.

In order to better examine the aerosol direct effect, this study focuses on clear-sky SW radiation in the following discussion. To further investigate the aerosol direct effect, the clear-sky direct and diffuse SW radiation is examined; annual mean time series and trends over the CONUS domain are plotted in Figs. 8c–f and 9c, d respectively. If the "brightening" effect is primarily caused by the anthropogenic aerosol direct effect, then in the absence of other forcing the clear-sky direct SW radiation should show an increasing trend while the clear-sky diffuse SW radiation would be expected to have a decreasing trend. However, in the observation, the clear-sky direct SW radiation shows no trend (i.e. very small increasing) while the clear-sky diffuse SW radiation has an increasing trend. In the simulation, the aerosol direct effects are clearly evident in the clear-sky direct and diffuse SW radiation (i.e. the results are the opposite of those in the observations, especially in the clear-sky diffuse radiation).

As shown in Table 5, the "brightening" occurs in the all-sky SW radiation while the cloudiness of both model and observations exhibit decreasing trends indicating the possibility that semi-indirect and/or indirect effects of decreasing aerosols may be a contributing factor. Aerosols can interact with clouds and precipitation in many ways, acting either as cloud condensation nuclei or ice nuclei, or as absorbing particles, redistributing solar energy as thermal energy inside cloud layers. In other words, decreasing troposphere burden of aerosol can cause decreasing of averaged cloud cover, and then this effect leads to more solar radiation reach to earth surface. However, trends in cloud cover can be influenced by many other factors which are very difficult to quantify based solely on available observational information. We also note that trends in both all-sky with (FB) and without (NFB) aerosol direct feedback for model prediction are very similar, but that the simulation with aerosol direct effect predicts a trend modestly closer to the observed trend in the eastern US (obs_east: 0.6296 $\mathrm{W\,m^{-2}\,year^{-1}}$, simFB_east: 0.4678 $\mathrm{W\,m^{-2}\,year^{-1}}$ and simNFB_east: 0.4148 $\mathrm{W\,m^{-2}\,year^{-1}}$) while the aerosol direct effect is less apparent in the

---

western US (obs_west: 0.5131 $\mathrm{W\,m^{-2}\,year^{-1}}$, simFB_west: 0.2389 $\mathrm{W\,m^{-2}\,year^{-1}}$, simNFB_west: 0.2877 $\mathrm{W\,m^{-2}\,year^{-1}}$). Implementing the aerosol indirect effect in the model may help to improve the simulation of all-sky SW total, direct and diffuse trends and this will be investigated in future analysis. Overall, the clear-sky SW radiation may be related at least in part with a decrease in aerosols, particularly in the eastern US where extensive reductions in the anthropogenic emissions of SO_2 and NO_x resulted from the implementation of CAA. This is further verified through the comparison of the feedback (FB) case with the no feedback (NFB) case which indicates almost no trends in the no feedback case in clear-sky total, direct and diffuse SW radiation (see Table 5). In contrast, the simulation with aerosol direct feedback effect show a clear association between decreasing aerosol burden with increasing clear-sky SW and also better agreement with trends in observed total SW. However, the comparison of the clear-sky diffuse SW radiation in the feedback case with the observations show that the radiative impacts of decreasing aerosol concentrations are confounded by other factors. As suggested by previous studies (Long et al., 2013; Augustine and Dutton, 2013; Gan et al., 2014a), some potential factors contributing to this discrepancy include increasing occurrences of contrail-generated ice haze that are caused by increasing air traffic producing an aggregate clear-sky "whitening" effect (a process missing in the current model), the traditional definition of "clear-sky" that allows a range of amount of condensed water in the column, and aerosol semi-direct and/or indirect effects. For example, as a result of the increasing air traffic, the contrails persistence and their moistening and aerosol emission in thin layers in the upper atmosphere (Hofmann et al., 1998) potentially producing ice haze layers can increase the diffuse radiation. Gan et al. (2014a) illustrate the pattern of US air carrier traffic (i.e. steady growth of air traffic from 1996 to 2007, followed by a decrease after 2008) which agreed well with the pattern inferred in the observed clear-sky diffuse radiation in particular the last 3 years (i.e. both of them decreased). Therefore it is important to characterize the properties of the contrail-generated ice haze (e.g. crystal shapes, ice layers and altitude) accurately. Haywood et al. (2009) and Gerritsen (2012) illustrate that increasing contrails do increase the diffuse radiation. This suggests that contrails or sub-visual cirrus clouds and ice haze can play a role in the increasing trend noted in the observed clear-sky diffuse SW radiation. However to capture this, characterizing the emission of air traffic and optical properties of the contrails realistically in the model is needed and will be pursued as part of a future study. It should also be noted that the methodology to retrieve clear-sky radiation from the measurements does not completely screen out condensed water in the atmospheric column similar to the traditional definition of "cloud-free" in sky imager retrievals and human observations (Long et al., 2009, 2006), and has been shown to include effects of sub-visual cirrus and cirrus haze (Dupont et al., 2008) that are still today included in the traditional "clear sky" definition. Additionally, the indirect/semi-direct aerosol and other cloud effects (Ruckstuhl et al., 2008) as well as the water vapor concentration (Haywood et al., 2011) can possibly impact the surface radiation. Thus, more investigation is needed to quantify and attribute the causes of the increase of measured clear-sky diffuse SW radiation.

4 Summary and conclusions

In general, the coupled WRF-CMAQ model is capable of replicating the observed trends in surface particulate matter concentration and AOD even though the magnitude of observed AOD is underestimated by the model. Possible causes of this underestimation could be under representation of some particulate matter constituent species in the model such as sea salt, organic carbon and other hygroscopic properties in the aerosol optics calculations, and uncertainties in the representation of the mixing state (Gan et al., 2014b; Curci et al., 2014). In particular, analysis of model and observations of clear-sky total SW trends during 2000–2010 agree well compared to those for 1995–2010, suggesting that the improved agreement for the more recent period may be due to the better estimates of recent emission dataset. This finding illustrates the importance of the accurate specification of the changes in emissions to capture the changes in aerosol burden and their radiative effects. Shortwave "brightening" trends

are apparent in both observations and model calculations for the past 16 years, though the magnitude is underestimated in the model. One purpose of using the modeling is to fill in the lack of spatial coverage of the observations, which in turn can help us to better understand the overall aerosol direct effects in the US.

Our analysis suggests an association between the SW radiation "brightening" (both all-sky and clear-sky) and troposphere aerosol burden over the past 16 years especially in the eastern US where large reductions in airborne particulate matter have occurred. Even though the "brightening" effect is underestimated in the clear-sky SW radiation in the model, it is still able to capture the total SW trend derived from the observations (i.e. both observation and model prediction illustrate increasing trends but smaller magnitude in the model), especially for the more recent years. Radiation trends in the western US could be influenced by local terrain influences as well as episodic long-range pollution transport which may contribute to the lack of a clear relationship between trends in aerosol burden and surface radiation at these locations. As a consequence of the CAA controls a dramatic reduction in particulate matter concentrations, especially SO_4^{2-} and NO_3^-, are found in the eastern US. Comparisons of modeled and observed clear-sky diffuse SW radiation shows that the radiative impacts of decreasing aerosol concentrations are confounded by other factors including: increasing ice deposition in the upper atmosphere from growing air traffic, differences in classification of "clear-sky" conditions between the radiation retrieval methodology and the model, differences in simulated cloudiness and aerosol semi-direct and indirect effects not represented in the current model simulations. In general, the representation of the trends in clear-sky and all-sky SW radiation in the simulation with aerosol direct effects relative to the observation are captured much better compared to the simulation without these effects. This indicates that at least a portion of trends in the recent radiation brightening, especially in the eastern US are influenced by decreasing aerosol levels in the region, which in turn have arisen from control of emissions of anthropogenic particulate matter and precursors species.

Acknowledgements. This research was performed while Chuen-Meei Gan held a National Research Council Research Associateship Award at US EPA. The research presented in this study was supported through an interagency agreement between the US Department of Energy (funding IA DE-SC0003782) and the US Environmental Protection Agency (funding IA RW-89–9233260). It has been subject to the US EPA's administrative review and approved for publication. The authors also would like thank John Augustine from NOAA-SURFRAD for his support and assistance in obtaining the SURFRAD data, as well as the NOAA Earth System Research Laboratory (ESRL) Global Monitoring Division (GMD) for their diligent efforts in operating and maintaining the SURFRAD sites. Long acknowledges the support of the Climate Change Research Division of the US Department of Energy as part of the Atmospheric Radiation Measurement (ARM) and Atmospheric System Research (ASR) Programs, and the support of the Cooperative Institute for Research in Environmental Sciences (CIRES). The authors would like thank James Kelly from US EPA for his comments.

References

Augustine, J. A. and Dutton, E. G.: Variability of the surface radiation budget over the United States from 1996 through 2011 from high-quality measurements, J. Geophys. Res.-Atmos., 118, 43–53, doi:10.1029/2012JD018551, 2013.

Blanchard, C. L., Hidy, G. M., Tanenbaum, S., Edgerton, E. S., and Hartsell. B. E.: The Southeastern Aerosol Research and Characterization (SEARCH) study: temporal trends in gas and PM concentrations and composition, 1999–2010, JAPCA J. Air Waste Ma., 63, 247–259, 2013.

Chin, M., Diehl, T., Tan, Q., Prospero, J. M., Kahn, R. A., Remer, L. A., Yu, H., Sayer, A. M., Bian, H., Geogdzhayev, I. V., Holben, B. N., Howell, S. G., Huebert, B. J., Hsu, N. C., Kim, D., Kucsera, T. L., Levy, R. C., Mishchenko, M. I., Pan, X., Quinn, P. K., Schuster, G. L., Streets, D. G., Strode, S. A., Torres, O., and Zhao, X.-P.: Multi-decadal aerosol variations from 1980 to 2009: a perspective from observations and a global model, Atmos. Chem. Phys., 14, 3657–3690, doi:10.5194/acp-14-3657-2014, 2014.

Curci, G., Hogrefe, C. Bianconi, R., Im, U., Balzarini, A., Baró, R., Brunner, D., Forkel, R., Giordano, L., Hirtl, M., Honzak, L., Jiménez-Guerrero, P., Knote, C., Langer, M., Makar, P. A., Pirovano, G., Pérez, J. L., San José, R., Syrakov, D., Tuccella, P., Werhahn, J., Wolke, R.,

Žabkar, R., Zhang, J., and Galmarini, S.: Uncertainties of simulated aerosol optical properties induced by assumptions on aerosol physical and chemical properties: an AQMEII-2 perspective, Atmos. Environ., in press, doi:10.1016/j.atmosenv.2014.09.009, 2014.

Gan, C.-M., Pleim, J., Mathur, R., Hogrefe, C., Long, C. N., Xing, J., Roselle, S., and Wei, C.: Assessment of the effect of air pollution controls on trends in shortwave radiation over the United States from 1995 through 2010 from multiple observation networks, Atmos. Chem. Phys., 14, 1701–1715, doi:10.5194/acp-14-1701-2014, 2014a.

Gan, C.-M., Binkowski, F., Pleim, J., Xing, J., Wong, D., Mathur, R., and Gilliam, R.: Assessment of the aerosol optics component of the coupled WRF-CMAQ model using CARES field campaign data and a single column model, Atmos. Environ., in press, doi:10.1016/j.atmosenv.2014.11.028, 2014b.

Gerritsen, K. O.: Case Study on the Effect of Aircraft Induced Cloudiness on the Short Wave Solar Irradiance at the Land Surface, Internship report of Earth System Science (ESS-70433), Royal Netherlands Meteorological Institute, available at: http://publicaties.minienm.nl/documenten/case-study-on-the-effect-of-aircraft-induced-cloudiness-on-the-s (last access: 29 June 2015), June 2012.

Hand, J. L., Schichtel, B. A., Malm, W. C., and Pitchford, M. L.: Particulate sulfate ion concentration and SO_2 emission trends in the United States from the early 1990s through 2010, Atmos. Chem. Phys., 12, 10353–10365, doi:10.5194/acp-12-10353-2012, 2012.

Hand, J. L., Schichtel, B. A., Malm, W. C., and Frank, N. H.: Spatial and temporal trends in $PM_{2.5}$ organic and elemental carbon across the United States, Adv. Meteorol., 2013, 367674, doi:10.1155/2013/367674, 2013.

Haywood, J. M., Allan, R. P., Bornemann, J., Forster, P. M., Francis, P. N., Milton, S., Rädel, G., Rap, A., Shine, K. P., and Thorpe, G.: A case study of the radiative forcing of persistent contrails evolving into contrail-induced cirrus, J. Geophys. Res., 114, D24201, doi:10.1029/2009JD012650, 2009.

Haywood, J. M., Bellouin, N., Jones, A., Boucher, O., Wild, M., and Shine, K. P.: The roles of aerosol, water vapor and cloud in future global dimming/brightening, J. Geophys. Res., 116, D20203, doi:10.1029/2011JD016000, 2011.

Hofmann, D. J., Stone, R., Wood, M. E., Deshler, T., and Harris, J. M.: An analysis of 25 years of balloon borne aerosol data in search of a signature of the subsonic commercial aircraft fleet, Geophys. Res. Lett., 25, 2433–2436, 1998.

Hogrefe, C., Pouliot, G., Wong, D., Torian, A., Roselle, S., Pleim, J., and Mathur, R.: Annual application and evaluation of the online coupled WRF-CMAQ system over North America under AQMEII phase 2, Atmos. Environ., in press, doi:10.1016/j.atmosenv.2014.12.034, 2014.

IPCC: Climate Change 2014: Impacts, Adaptation, and Vulnerability, Part A: Global and Sectoral Aspects, Contribution of Working Group II to the Fifth Assessment Report of the Intergovernmental Panel on Climate Change, edited by: Field, C. B., Barros, V. R., Dokken, D. J., Mach, K. J., Mastrandrea, M. D., Bilir, T. E., Chatterjee, M., Ebi, K. L., Estrada, Y. O., Genova, R. C., Girma, B., Kissel, E. S., Levy A. N., MacCracken, S., Mastrandrea, P. R., and White, L. L., Cambridge University Press, Cambridge, UK, New York, NY, USA, 1132 pp., 2014a.

IPCC: Climate Change 2014: Impacts, Adaptation, and Vulnerability, Part B: Regional Aspects, Contribution of Working Group II to the Fifth Assessment Report of the Intergovernmental Panel on Climate Change, , edited by: Barros, V. R., Field, C. B., Dokken, D. J., Mach, K. J., Mastrandrea, M. D., Bilir, T. E., Chatterjee, M., Ebi, K. L., Estrada, Y. O., Genova, R. C., Girma, B., Kissel, E. S., Levy A. N., MacCracken, S., Mastrandrea, P. R., and White, L. L., Cambridge University Press, Cambridge, United Kingdom and New York, NY, USA, 688 pp., 2014b.

Long, C. N., Sabburg, J. M., Calbo, J, and Page, D.: Retrieving cloud characteristics from ground-based daytime color all-sky images, J. Atmos. Ocean. Tech., 23, 633–652, 2006.

Long, C. N., Dutton, E. G., Augustine, J. A., Wiscombe, W., Wild, M., McFarlane, S. A., and Flynn, C. J.: Significant decadal brightening of downwelling shortwave in the continental United States, J. Geophys. Res., 114, D00D06, doi:10.1029/2008JD011263, 2009.

Pleim, J. E. and Gilliam, R.: An indirect data assimilation scheme for deep soil temperature in the Pleim–Xiu land surface model, J. Appl. Meteorol. Clim., 48, 1362–1376, 2009.

Pleim, J. E. and Xiu, A.: Development of a land surface model, Part II: Data assimilation, J. Appl. Meteorol., 42, 1811–1822, 2003.

Ruckstuhl, C., Philipona, R., Behrens, K., Coen, C. M., Durr, B., Heimo, A. Matzler, C., Nyeki, S., Ohmura, A., Vuilleumier, L., Weller, M., Wehrli, C., and Zelenka, A.: Aerosol and cloud effects on solar brightening and the recent rapid warming, Geophys. Res. Lett., 35, L12708, doi:10.1029/2008GL034228, 2008.

Stauffer, R. D. and Seaman, L. N.: Multiscale four-dimensional data assimilation, J. Appl. Meteorol., 33, 416–434, doi:10.1175/1520-0450(1994)033<0416:MFDDA>2.0.CO;2, 1994.

Wild, M., Trüssel, B., Ohmura, A., Long, C. N., König-Langlo, G., Dutton, E. G., and Tsvetkov, A.: Global dimming and brightening: an update beyond 2000, J. Geophys. Res., 114, D00D13, doi:10.1029/2008JD011382, 2009.

Wong, D. C., Pleim, J., Mathur, R., Binkowski, F., Otte, T., Gilliam, R., Pouliot, G., Xiu, A., Young, J. O., and Kang, D.: WRF-CMAQ two-way coupled system with aerosol feedback: software development and preliminary results, Geosci. Model Dev., 5, 299–312, doi:10.5194/gmd-5-299-2012, 2012.

Xing, J., Pleim, J., Mathur, R., Pouliot, G., Hogrefe, C., Gan, C.-M., and Wei, C.: Historical gaseous and primary aerosol emissions in the United States from 1990 to 2010, Atmos. Chem. Phys., 13, 7531–7549, doi:10.5194/acp-13-7531-2013, 2013.

Xing, J., Mathur, R., Pleim, J., Hogrefe, C., Gan, C.-M., Wong, D. C., Wei, C., Gilliam, R., and Pouliot, G.: Observations and modeling of air quality trends over 1990–2010 across the Northern Hemisphere: China, the United States and Europe, Atmos. Chem. Phys., 15, 2723–2747, doi:10.5194/acp-15-2723-2015, 2015.

Yu, S., Mathur, R., Pleim, J., Wong, D., Gilliam, R., Alapaty, K., Zhao, C., and Liu, X.: Aerosol indirect effect on the grid-scale clouds in the two-way coupled WRF–CMAQ: model description, development, evaluation and regional analysis, Atmos. Chem. Phys., 14, 11247–11285, doi:10.5194/acp-14-11247-2014, 2014.

Table 1. Listing of site identification of each site for different networks and their measurement period which are used in this study. Distance means the approximate distance between SURFRAD/ARM sites with CASTNET or IMPROVE sites.

SURFRAD/ARM	SW Radiation	AOD	CASTNET	Aerosol Concentration	IMPROVE	Aerosol Concentration
PSU [Penn State, PA] Elevation: 0.38 km Lat: 40.72° Lon: −77.93°	1999–2010	1999–2009	PSU106 [Penn State, PA] Distance: 0 km Elevation: 0.38 km Lat: 40.72° Lon: −77.93°	1990–2010	WASH1 [Washington DC] Distance: 210 km Elevation: 0.02 km Lat: 38.88° Lon: −77.03°	1990–2010
BON [Bondville, IL] Elevation: 0.23 km Lat: 40.05° Lon: −88.37°	1995–2010	1997–2010	BVL130 [Bondville, IL] Distance: 0 km Elevation: 0.21 km Lat: 40.05° Lon: −88.37°	1990–2010	BONL1 [Bondville, IL] Distance: 0 km Elevation: 0.21 km Lat: 40.05° Lon: −88.37°	2001–2010
GWN [Goodwin Creek, MS] Elevation: 0.1 km Lat: 34.25° Lon: −89.87°	1995–2010	1997–2010	CVL151 [Coffeeville, MS] Distance: 30 km Elevation: 0.1 km Lat: 34.00° Lon: −89.80°	1990–2010	MACA1 [Mammoth Cave NP, KY] Distance: 500 km Elevation: 0.25 km Lat: 37.13° Lon: −86.15°	1992–2010
SGP [South Great Plain, OK] Elevation: 0.31 km Lat: 36.80° Lon: −97.50°	1997–2010	1996–2007	CHE185 [Cherokee, OK] Distance: 270 km Elevation: 0.3 km Lat: 35.75° Lon: −94.67°	2002–2010	CHER1 [Cherokee Nation, OK] Distance: 50 km Elevation: 0.34 km Lat: 36.93° Lon: −97.02°	2003–2010
FPK [Fort Peck, MT] Elevation: 0.63 km Lat: 48.31° Lon: −105.10°	1996–2010	1997–2010	THR422 [Theodore, ND] Distance: 170 km Elevation: 0.85 km Lat: 46.89° Lon: −103.38°	1998–2010	MELA1 [Midicine Lake, MT] Distance: 50 km Elevation: 0.61 km Lat: 48.49° Lon: −104.48°	2000–2010
TBL [Table Mountain, CO] Elevation: 1.69 km Lat: 40.13° Lon: −105.24°	1996–2010	1997–2010	ROM406 [Rocky Mtn NP, CO] Distance: 30 km Elevation: 2.7 km Lat: 40.28° Lon: −105.55°	1994–2010	ROMO1 [Rocky Mountain NP, CO] Distance: 30 km Elevation: 2.8 km Lat: 40.28° Lon: −105.55°	1991–2008
DRA [Desert Rock, NV] Elevation: 1.01 km Lat: 36.63° Lon: −116.02°	1999–2010	1999–2010	DEV412 [Death Valley, CA] Distance: 85 km Elevation: 0.12 km Lat: 36.51° Lon: −116.85°	1995–2007	DEVA1 [Death Valley NP, CA] Distance: 85 km Elevation: 0.13 km Lat: 36.51° Lon: −116.85°	2000–2010

Table 2. List of configurations.

Parameter	Configuration
Emission	Xing et al. (2013)
Planetary Boundary Layer	ACM2 Pleim (2007)
Microphysics	Morrison 2-moment
Gas-phase Chemistry	Carbon Bond 05
Aerosol Chemistry	Carbon Bond 05
Surface layer	Pleim–Xiu
Cumulus	Kain-Fritsch (new Eta)
Radiation	RRTMG SW & LW
Land use	NLCD 50
Boundary condition	Hemisphere run from Xing et al. (2015)

Table 3. Trends of 16 years for CASTNET, aerosol feedback (FB) simulation and emission.

CASTNET			East			
		observation			simulation (FB)	
(µg m^{-3})	trend	significance	confident	trend	significance	confident
SO_4^{2-}	−0.1346	23.8675	> 95	−0.1115	34.8830	> 95
SO_2	−0.2089	19.4757	> 95	−0.2624	33.7830	> 95
NO_3^-	−0.1026	30.4293	> 95	−0.0348	18.5530	> 95
CASTNET			West			
		observation			simulation (FB)	
(µg m^{-3})	trend	significance	confident	trend	significance	confident
SO_4^{2-}	−0.0026	2.5329	> 95	0.0010	1.8118	> 90
SO_2	−0.0121	10.3122	> 95	−0.0108	28.0550	> 95
NO_3^-	−0.1100	10.7925	> 95	−0.0052	14.9930	> 95
		East emission			West emission	
(mole s^{-1} m^{-2})	trend	significance	confident	trend	significance	confident
SO_2	−0.0792	49.0140	> 95	−0.0102	29.5820	> 95
NO_x	−0.0636	140.7900	> 95	−0.0522	21.4980	> 95

Table 4. Trends of 16 years for IMPROVE, aerosol feedback (FB) simulation and emission.

IMPROVE			East			
		observation			simulation (FB)	
(µg m^{-3})	trend	significance	confident	trend	significance	confident
SO_4^{2-}	−0.0933	13.1013	> 95	−0.1358	47.3720	> 95
NO_3^-	0.0025	0.3906	< 90	−0.0585	28.9020	> 95
EC	−0.0106	7.7710	> 95	−0.0195	24.6109	> 95
$PM_{2.5}$	−0.2998	26.3410	> 95	−0.4419	61.3020	> 95
IMPROVE			West			
		observation			simulation (FB)	
(µg m^{-3})	trend	significance	confident	trend	significance	confident
SO_4^{2-}	0.0038	4.3870	> 95	−0.0006	1.3370	< 90
NO_3^-	0.0069	5.3737	> 95	−0.0078	19.0980	> 95
EC	−0.0033	26.1560	> 95	−0.0001	0.2313	< 90
$PM_{2.5}$	0.0181	2.4442	> 95	−0.0151	4.0741	> 95
		East emission			West emission	
(mole s^{-1} m^{-2})	trend	significance	confident	trend	significance	confident
SO_2	−0.0941	7.9968	> 95	−0.0102	29.5810	> 95
NO_x	−0.1628	42.8840	> 95	−0.0519	21.4580	> 95
EC	−0.0889	29.6640	> 95	−0.0090	2.7338	> 95

Table 5. Trends of 16 years for SURFRAD, aerosol feedback (FB) and without feedback (NFB) simulations.

SURFRAD					East				
		observation			simulation (FB)			simulation (NFB)	
	trend	significance	confident	trend	significance	confident	trend	significance	confident
SW ($\mathrm{W\,m^{-2}\,year^{-1}}$)	0.6296	11.1315	> 95	0.4678	9.8347	> 95	0.4148	7.5757	> 95
SWC ($\mathrm{W\,m^{-2}\,year^{-1}}$)	0.3691	12.6481	> 95	0.1242	12.5670	> 95	0.0006	0.1786	< 90
SW DIR ($\mathrm{W\,m^{-2}\,year^{-1}}$)	0.4149	7.2066	> 95	0.8364	11.2120	> 95	0.6817	7.3320	> 95
SW DIF ($\mathrm{W\,m^{-2}\,year^{-1}}$)	0.2555	10.8605	> 95	−0.3589	13.3040	> 95	−0.2586	7.1687	> 95
SWC DIR ($\mathrm{W\,m^{-2}\,year^{-1}}$)	−0.0085	0.2701	< 90	0.5810	23.7720	> 95	0.0038	0.9496	< 90
SWC DIF ($\mathrm{W\,m^{-2}\,year^{-1}}$)	0.3764	35.1138	> 95	−0.4569	32.0910	> 95	−0.0031	5.9625	> 95
AOD (unitless)	−0.0012	4.2559	> 95	−0.0017	30.7585	> 95			
Cloudiness (unitless)	−0.0021	6.1257	> 95	−0.0034	7.6943	> 95			
SURFRAD					West				
		observation			simulation (FB)			simulation (NFB)	
	trend	significance	confident	trend	significance	confident	trend	significance	confident
SW ($\mathrm{W\,m^{-2}\,year^{-1}}$)	0.5131	14.2751	> 95	0.2389	6.4364	> 95	0.2877	7.9451	> 95
SWC ($\mathrm{W\,m^{-2}\,year^{-1}}$)	0.4799	10.8243	> 95	0.0148	1.0263	< 90	0.0506	8.1029	> 95
SW DIR ($\mathrm{W\,m^{-2}\,year^{-1}}$)	0.1739	3.5616	> 95	0.4648	10.0480	> 95	0.6432	12.5980	> 95
SW DIF ($\mathrm{W\,m^{-2}\,year^{-1}}$)	0.4009	8.2052	> 95	−0.2204	15.0360	> 95	−0.3414	15.9440	> 95
SWC DIR ($\mathrm{W\,m^{-2}\,year^{-1}}$)	0.0005	0.0148	< 90	−0.0758	3.3132	> 95	0.0493	8.0979	> 95
SWC DIF ($\mathrm{W\,m^{-2}\,year^{-1}}$)	0.4781	18.8751	> 95	0.0906	8.1834	> 95	0.0014	0.6051	< 90
AOD (unitless)	0.0009	6.7010	> 95	0.0001	1.1083	< 90			
Cloudiness (unitless)	−0.0012	2.7129	> 95	−0.0031	13.0811	< 90			

SW: All-sky shortwave radiation; SWC: Clear-sky shortwave radiation; DIR: direct; DIF: diffuse; AOD: aerosol optical depth.

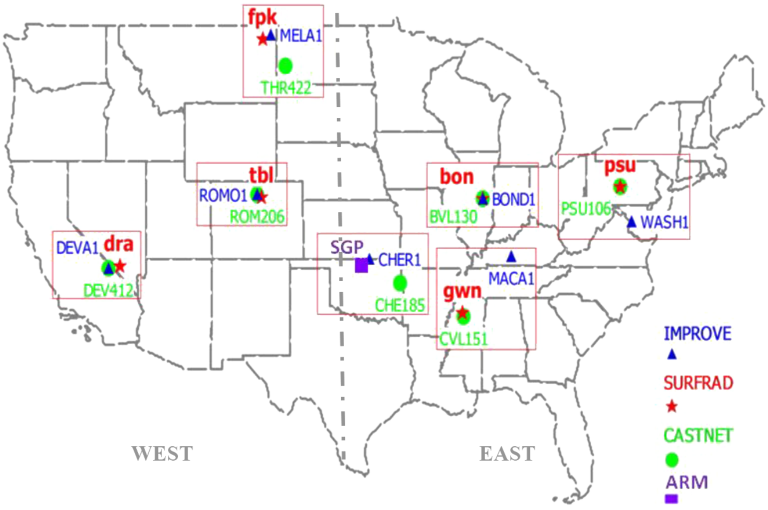

Figure 1. Locations of various sites in SURFRAD, ARM, CASTNET and IMPROVE networks.

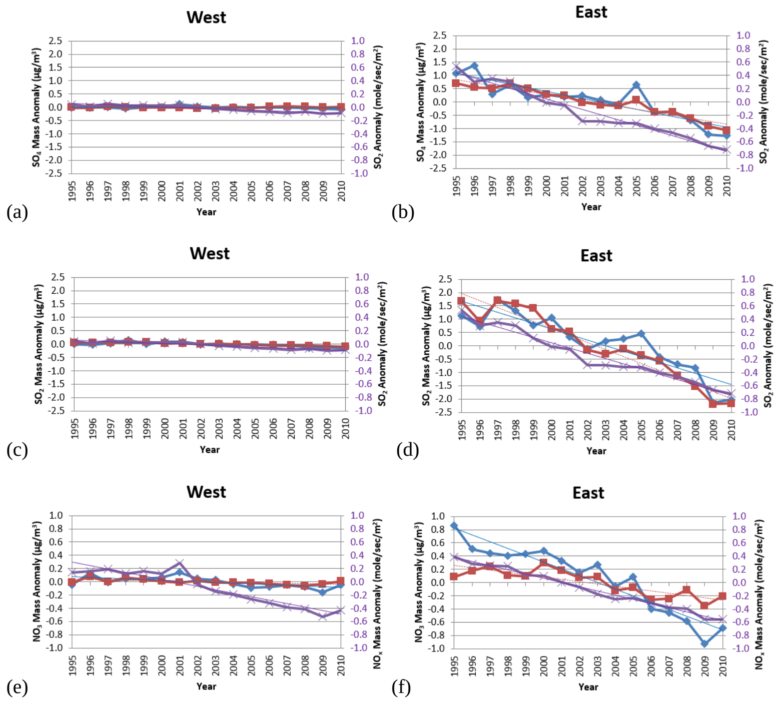

(a) (b) (c) (d) (e) (f)

Figure 2. Annual mean anomalies of 1995–2010 SO_4^{2-} (1st row), SO_2 (2nd row) and NO_3^- (3rd row) for CASTNET observations (blue line – primary *y* axis), model simulations (red line – primary *y* axis) and emissions (purple line – secondary *y* axis). Least-square fit trend lines are also shown for each time series. Note that for emission dataset, only SO_2 (paired with SO_2 and SO_4^{2-}) and NO_x (paired with NO_3^-) are available. The left column represents the western US while the right column represents the eastern US.

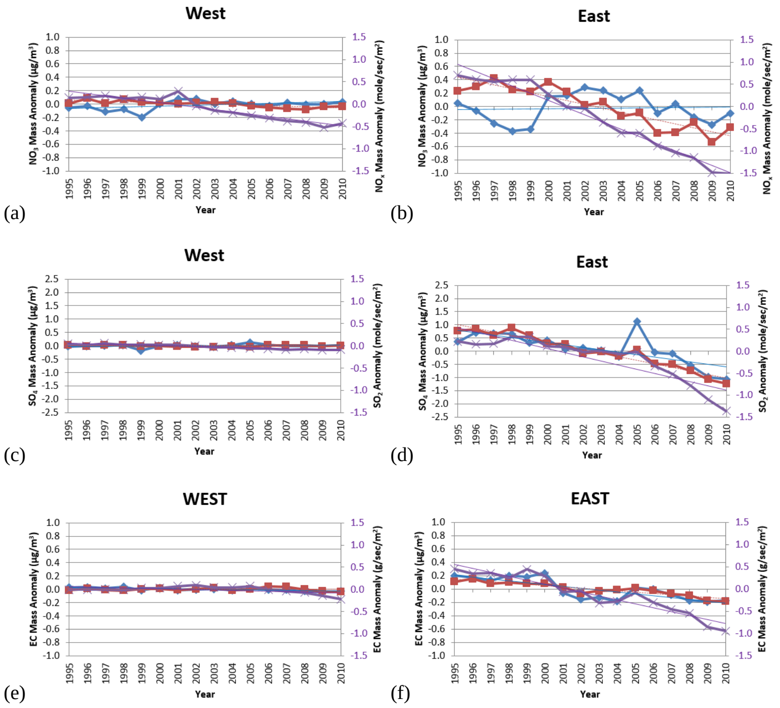

(a) (b) (c) (d) (e) (f)

Figure 3. Annual mean anomalies of 1995–2010 SO_4^{2-} (1st row), NO_3^- (2nd row) and EC (3rd row) for IMPROVE observation (blue line – primary *y* axis), model simulations (red line – primary *y* axis) and emissions (purple line – secondary *y* axis). Least-square fit trend lines are also shown for each time series. Note that for emission dataset, only SO_4^{2-}, (paired with SO_2) and NO_x (paired with NO_3^-) are available. The left column represents the western US while the right column represents the eastern US.

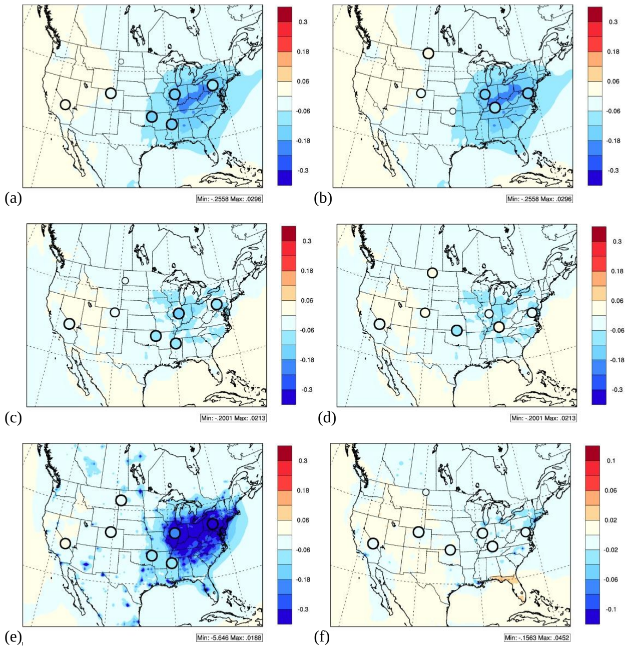

(a) (b)

(c) (d)

(e) (f)

Figure 4. Map of annual trends based on 1995–2010 coupled WRF-CMAQ simulations over the CONUS domain are depicted along with circles representing observed trends for seven sites. Left column for SO_4^{2-} (1st row), NO_3^- (2nd row) and SO_2 (3rd row) from CASTNET network while the right column if for SO_4^{2-} (1st row), NO_3^- (2nd row) and EC (3rd row) from IMPROVE network. Note that the size of the circle represents the level of the significance. Larger circle means more significance.

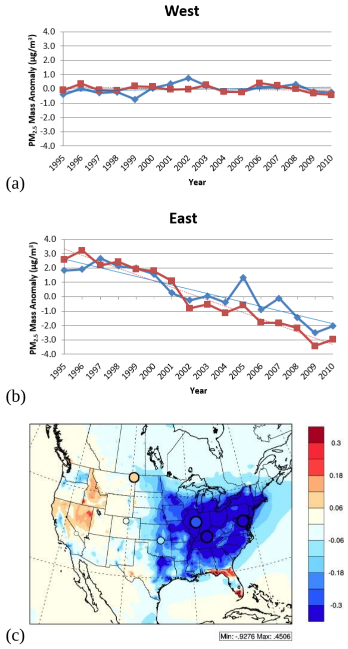

(a)

(b)

(c)

Figure 5. Annual mean anomalies of 1995–2010 $PM_{2.5}$ **(a)** western and **(b)** eastern US from IMPROVE for observations (blue line) and model simulations (red line). Least-square fit trend lines are also shown for each time series. **(c)** Map of $PM_{2.5}$ annual trends based on 1995–2010 coupled WRF-CMAQ simulations over the CONUS domain are depicted along with circles representing observed trends for seven sites. Note that the size of the circle represents the level of the significance. Larger circle means more significance.

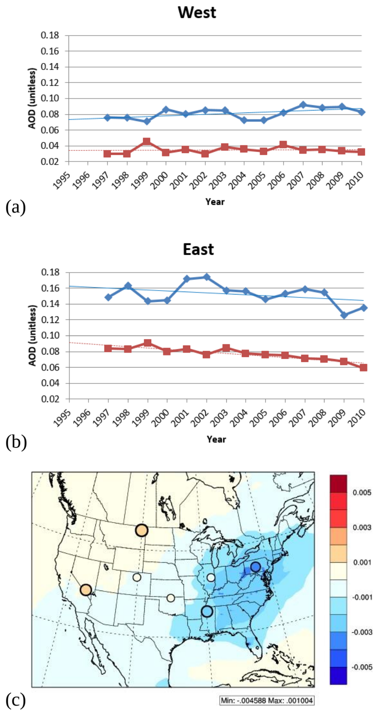

Figure 6. Annual mean of 1997–2010 AOD **(a)** western and **(b)** eastern US from SURFRAD for observation (blue line) and model simulations (red line). Least-square fit trend lines are also shown for each time series. **(c)** Map of AOD annual trends based on 1995–2010 coupled WRF-CMAQ simulations over the CONUS domain are depicted along with circles representing observed trends for seven sites. Note that the size of the circle represents the level of the significance. Larger circle means more significance.

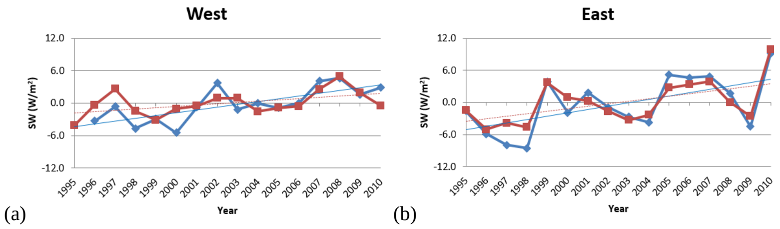

Figure 7. Annual mean anomalies of 1995–2010 all-sky total SW radiation for SURFRAD observations (blue line) and model simulations (red line). Least-square fit trend lines are also shown for each time series. The left column represents the western US while the right column represents the eastern US.

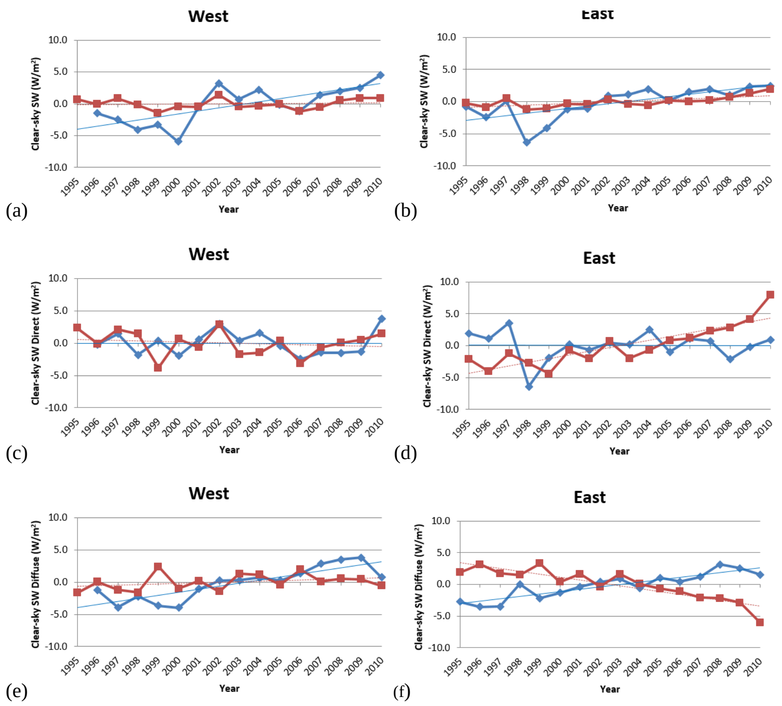

Figure 8. Annual mean anomalies of clear-sky total (1st row), direct (2nd row) and diffuse (3rd row) SW radiation for SURFRAD observation (blue line) and model 16 years (red) together with their trends respectively. The left column represents the western US while the right column represents the eastern US.

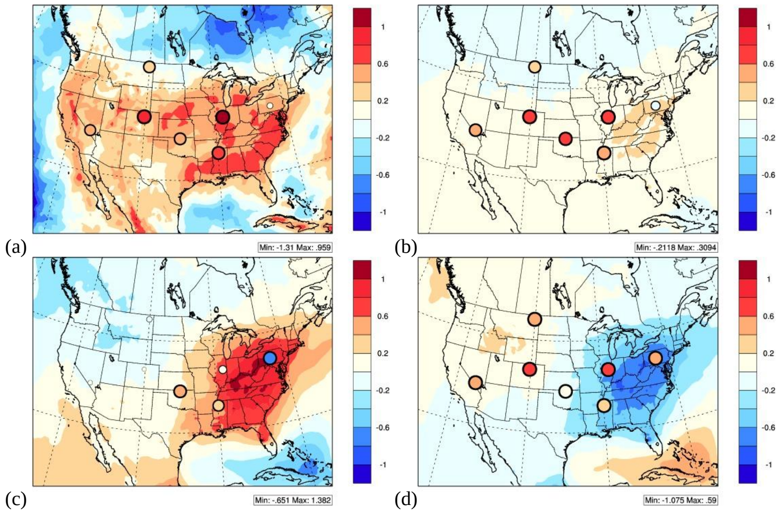

Figure 9. Map of annual trends based on 1995–2010 coupled WRF-CMAQ simulations over the CONUS domain for **(a)** all-sky total SW radiation, **(b)** clear-sky total SW radiation, **(c)** clear-sky direct SW radiation and **(d)** clear-sky diffuse SW radiation are depicted along with circles representing SURFRAD observed trends for seven sites. Note that the size of the circle represents the level of the significance. Larger circle means more significance.